NANO LETTERS

Letter

Cite This: Nano Lett. 2017, 17, 6690-6695

pubs.acs.org/NanoLett

Millimeter-Scale Spatial Coherence from a Plasmon Laser

Thang B. Hoang,[†,‡,#] Gleb M. Akselrod,[†,§] Ankun Yang,[∥,▽] Teri W. Odom,[∥,⊥] and Maiken H. Mikkelsen*[,†,‡,§]

[†]Center for Metamaterials and Integrated Plasmonics, [‡]Department of Physics, and [§]Department of Electrical and Computer Engineering, Duke University, Durham, North Carolina 27708, United States

[∥]Department of Materials Science and Engineering and [⊥]Department of Chemistry, Northwestern University, Evanston, Illinois 60208, United States

Supporting Information

ABSTRACT: Coherent light sources have been demonstrated based on a wide range of nanostructures, however, little effort has been devoted to probing their underlying coherence properties. Here, we report long-range spatial coherence of lattice plasmon lasers constructed from a periodic array of gold nanoparticles and a liquid gain medium at room temperature. By combining spatial and temporal interferometry, we demonstrate millimeter-scale (~1 mm) spatial coherence and picosecond (~2 ps) temporal coherence. The long-range spatial coherence occurs even without the presence of strong coupling with the lattice plasmon mode extending over macroscopic distances in the lasing regime. This plasmonic lasing system thus provides a platform for understanding the emergence of long-range coherence from collections of nanoscale resonators and points toward novel types of distributed lasing sources.

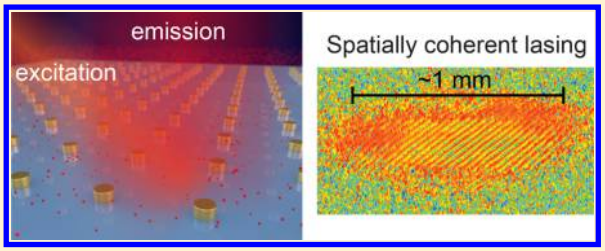

KEYWORDS: *Plasmonics, nanolasers, temporal coherence, spatial coherence*

Lasing, a result of stimulated emission, has long been demonstrated in various nanostructures, including solid state nanocavities,[1−4] photonic cavities,[5−7] disordered media,[8] and plasmonic structures,[9−18] employing both inorganic and organic active media. These subwavelength light sources are energy efficient, tunable, and capable of on-chip integration.[19,20] Characteristics of a lasing structure include a pumping threshold associated with the narrowing of the spectral line width, indicating a transition from spontaneous emission to stimulated emission. Most studies on nanolaser systems are limited to demonstrations of these basic characteristics, while a few recent studies have verified coherent light emission through either second-order correlation measurements[17] or by observation of distinct interference patterns arising from the two ends of a semiconductor nanowire laser.[3] However, despite intense interest in nanostructured lasers, measurements of their essential temporal and spatial coherence lengths, which ultimately define the quality of a lasing source and determine the directionality and spectral line width of the source, remains an outstanding challenge. By contrast, spatial and temporal coherence have been widely investigated in various systems that support polariton condensation, a state in which the photonic mode of the cavity is strongly coupled to the gain medium. One of the most striking features of coherence in lasing and condensate systems is the appearance of spatial coherence above the nonlinear threshold. First-order spatial coherence is characterized by phase correlations between emitted photons from spatially separated parts of the structure. Spatial coherence has been observed in polaritonic microcavities showing Bose−Einstein condensation (BEC) behavior with typical coherence lengths of 10−15 μm for inorganic gain layers[21,22] and up to 40 μm for organic gain layers.[23,24] Despite the much studied polaritonic systems, understanding of the spatial and temporal coherence properties is lacking for nanostructured lasing systems.

In this article, we experimentally probe both the temporal and spatial coherence properties of a plasmon nanolaser based on periodic arrays of metallic nanoparticles immersed in a liquid gain medium. These plasmonic arrays possess band-edge lattice modes that are delocalized over many lattice periods and coherently interact with localized hot spot regions surrounding the nanoparticles where the population inversion occurs. The large volume of this mode therefore promotes coupling between the lasing field and the free-space field due to a small momentum mismatch.[10,12] Using spatial and temporal interferometry we show that this lasing mode exhibits coherence over a macroscopic length scale (~1 mm). Even in the absence of strong coupling, we observe this extreme long-range spatial coherence that is more than an order of magnitude greater than has been observed for condensate systems.

The plasmon laser consists of an array of gold nanoparticles situated on a fused silica substrate (Figure 1a). Figure 1b displays an SEM image of the nanoparticle array as well as a

Received: June 25, 2017
Revised: September 20, 2017
Published: September 28, 2017

DOI: 10.1021/acs.nanolett.7b02677
Nano Lett. 2017, 17, 6690−6695

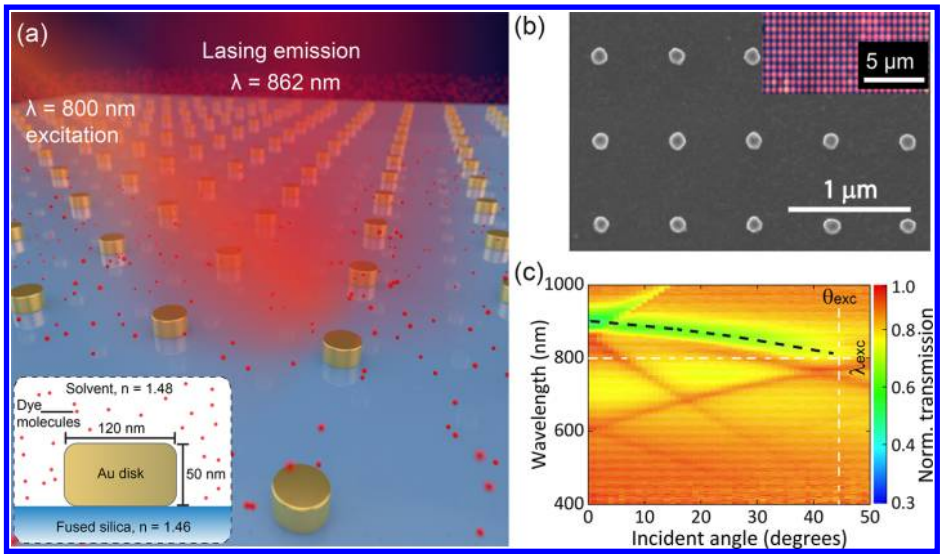

Figure 1. Plasmon nanolaser. (a) Illustration of the nanoparticle array laser with the excitation beam and emission beam delocalized over many nanoparticles. Inset: Cross-sectional schematic of a single gold nanoparticle surrounded by the DMSO solution containing IR-140 dye molecules. (b) SEM image of the gold nanoparticle array. Inset: dark-field optical image of the sample with individual nanoparticles visible. (c) Photonic band diagram measured by angle-resolved transmission for the case with DMSO solvent and 1 mM IR-140 dye present. The white dashed lines indicate the incident angle and wavelength of the laser excitation. Transmitted light was normalized by the IR-140 dye absorption (see Supporting Information Figure S1c). The black dashed line is a guide to the eye of the band-edge lattice plasmon that follows the $(0, \pm 1)$ mode.

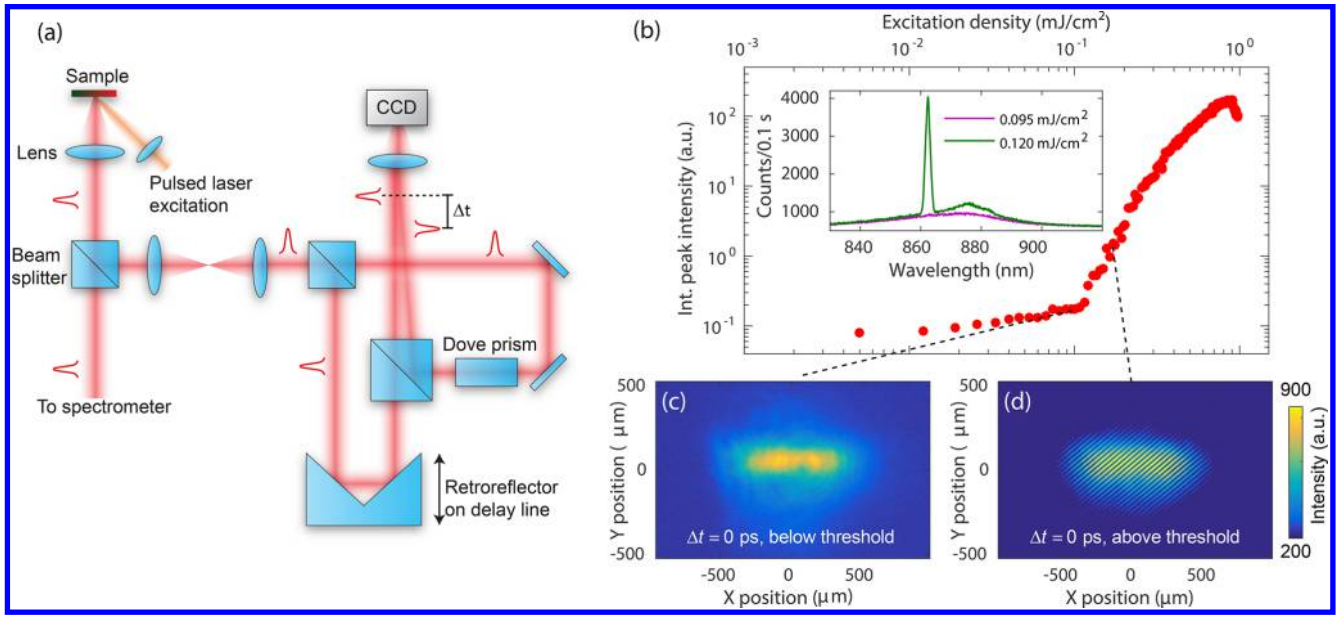

Figure 2. Measurements of coherence properties. (a) Schematic of the experimental setup utilizing a modified Michelson interferometer. The sample was mounted such that the symmetry axes of the nanoparticle lattice aligned with the horizontal and vertical directions. (b) Excitation power dependence of the spectrally integrated emission intensity showing a clear threshold ~0.11 mJ/cm^2. Inset shows emission spectra at various excitation densities. (c) CCD camera image of the emission right below the lasing threshold at an excitation power of P = 0.10 mJ/cm^2, a delay time of Δt = 0 ps and with the beams from the two arms of the interferometer spatially overlapped. (d) Same measurement as in (c) but at a higher excitation power of P = 0.15 mJ/cm^2 above the lasing threshold resulting in a clear interference pattern.

dark-field optical image of the sample. The gold nanoparticle array is covered by a liquid gain medium containing index matching dimethyl sulfoxide (DMSO) solvent with refractive index n = 1.48 and IR-140 dye molecules at a concentration of 1 mM and held in place by a top glass coverslip. The band-edge lattice plasmon resonance of the nanoparticle array can support lasing action in the direction perpendicular to the sample surface.[10,11] The resonance wavelength can be tuned by adjusting the nanoparticle size or lattice spacing[10] or by dynamically varying the liquid gain medium.[11]

One key question to answer when studying the coherence characteristics of a system showing nonlinear emission is whether it is an exciton−polariton condensate operating in the strong coupling regime[23−29] or a laser operating in the weak coupling regime.[30] To clarify whether strong coupling is present in our system, we first investigate the photonic band structure of the nanoparticle array with and without the IR-140

DOI: 10.1021/acs.nanolett.7b02677
Nano Lett. 2017, 17, 6690−6695

dye molecules. In agreement with previous studies,[10,11] when only the DMSO solvent is present, the lattice plasmon resonances under unpolarized light exhibit several dispersive bands that follow the Rayleigh anomaly modes (Supporting Information Figure S1a). With the addition of the dye (Figure 1c), the band structure of the lattice plasmon mode is still clearly observed and is not strongly modified by the presence of the dye. Therefore, in the presence of gain medium the system does not exhibit any indication of strong coupling, as expected from the low dye concentration.[31]

To measure the spatial and temporal coherence we utilize a modified Michelson interferometer that combines a retroreflector configuration[22] with an ultrashort pulsed laser temporal coherence measurement technique.[32] Figure 2a shows the schematic of our experimental setup where the sample was pumped by an 800 nm, 150 fs, 1 kHz Ti:Sa laser at an incident angle of 45° and with a ∼ 1 mm spot size. The lasing signal from the sample was collected normal to the sample surface through a 5× objective and split by a beam splitter for either spectral measurements on a spectrometer and charge-coupled device (CCD) camera connected via a single mode fiber or for coherence measurements performed using free space coupling. For the coherence measurements, the signal was further divided into two different paths. The first path was sent through a retroreflector on a mechanical delay line, and the second path went through a Dove prism which allows for the real image to be rotated with respect to the optical axis. For the measurements of temporal coherence, the Dove prism was oriented such that the real images on both arms were overlapped exactly.

Figure 2b displays the integrated emission intensity as a function of the pump density, which exhibits a clear threshold at an excitation density of P_{th} = 0.11 mJ/cm^2. At low excitation density, the dye molecule emission is characterized by a broad spontaneous emission spectrum, and as the excitation density increases, a narrow stimulated emission peak appears at ∼862 nm with a full width at half-maximum (fwhm) of 1.6 nm. At high excitation densities (>1 mJ/cm^2), the integrated emission intensity decreases rapidly, resulting from the emergence of amplified spontaneous emission (ASE)[10,33] as well as direct dye bleaching. Furthermore, no blue-shift is observed in the emission spectrum with increasing power, in contrast to polaritons in strongly interacting systems,[23,25] further confirming the absence of strong coupling. Figure 2c,d shows the CCD images of the emission at excitation densities below and above the lasing threshold where the two arms are overlapped in time (Δt = 0) and space. As expected, an interference pattern only occurs above the lasing threshold indicating the onset of coherent emission from the structure. We note that the ASE in our system[10,11] can only be seen at off-normal angles determined by the dispersion relation of the lattice plasmons and emerges at higher excitation powers as a distinct, broader peak.[10]

To characterize the temporal coherence, we measured the interference patterns at different delay times, Δt, between the two paths (Figure 3a). When the two paths overlapped exactly in both space and time (Δt = 0 ps), a maximum fringe visibility of the interference pattern occurred. To quantify the coherence time, a series of CCD images were collected and Fourier transformed. We then extracted the magnitudes of the spatial frequencies corresponding to the interference fringes in the Fourier space and plotted these magnitudes against the relative delay times. Figure 3b displays the data from two different

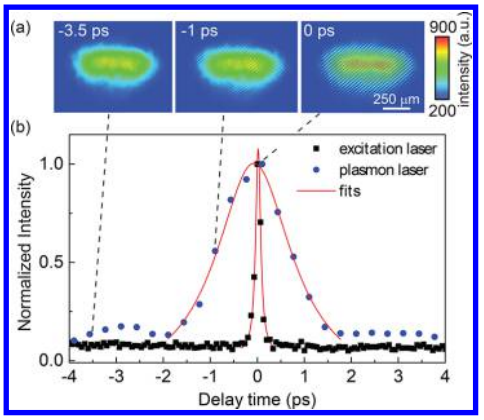

Figure 3. Measurements of temporal coherence. (a) Real-space CCD images acquired at different delay times, Δt = −3.5,−1.0, and 0 ps, and at an excitation density above the lasing threshold of P = 1.5 P_{th}. (b) Magnitudes of the Fourier transformed spatial frequency at different delay times for the plasmon laser (blue, circle) and for the commercial excitation laser (black, square) as a control measurement. The extracted fwhm from fits to the data (red solid lines) were 2.0 and 0.16 ps for the plasmon and excitation laser, respectively.

experiments: (1) lasing from a plasmon laser (blue circles), and (2) measurement of the pump laser itself (back squares) as a control. In both cases, a distinct peak appears at a relative delay time of Δt = 0 ps, and the fwhm of this peak represents the coherence time.[32] As expected, the pump laser exhibited a narrow peak with a fwhm of ∼0.16 ± 0.01 ps, very close to the manufacturer specified value of 0.15 ps (see also Supporting Information Figure S3). Meanwhile, the plasmon laser shows temporal coherence with a fwhm of 2.0 ± 0.2 ps. As seen in the inset of Figure 2b, the plasmon laser was characterized by a narrow lasing peak with a line width of ∼1.6 nm, and from the relation $\tau_{coherence} = \lambda^2/(c\Delta\lambda)$, where λ is the wavelength, $\Delta\lambda$ is the line width, and c is the speed of light, we can estimate a coherence time of $\tau_{coherence}$ = 1.55 ps which is close to the value extracted from the interference measurement. Finally, we note that the technique used here is equivalent to measuring the visibility $V = (I_{max} - I_{min})/(I_{max} + I_{min})$, where I_{max} and I_{min} are the maximum and minimum intensities of the interference fringes at various delay times.[24,32]

Following the measurement technique developed for spatial coherence studies of strongly interacting systems,[21−24] we measured the spatial correlation function $g^1(\mathbf{r}, -\mathbf{r})$ of the lattice plasmon laser. To do this, the real-space image on one arm of the interferometer was rotated by a Dove prism such that the two arms are spatially inverted and overlapped in a centro-symmetrical way (Figure 4a and Supporting Information Figure S4). As the emission from the structure is elongated along the incident polarization axis,[10,11] in the following experiments the excitation laser is vertically polarized, instead of horizontally, to minimize any time delay between the two ends of the excitation spot.

Figure 4a displays a typical interference image and the center region of interest is shown below in Figure 4b for different delay times with the black dot indicating the same pixel on the camera. By tracing the intensity of this pixel at different time delays, an interference fringe is obtained (Figure 4c) from which the visibility, V, can be calculated. To reconstruct both the spatial correlation function, $g^1(\mathbf{r}, -\mathbf{r})$, and the related phase, the interference fringe obtained from each pixel in Figure 4a has been fit with a cosine function,[21,24] and the results

DOI: 10.1021/acs.nanolett.7b02677
Nano Lett. 2017, 17, 6690−6695

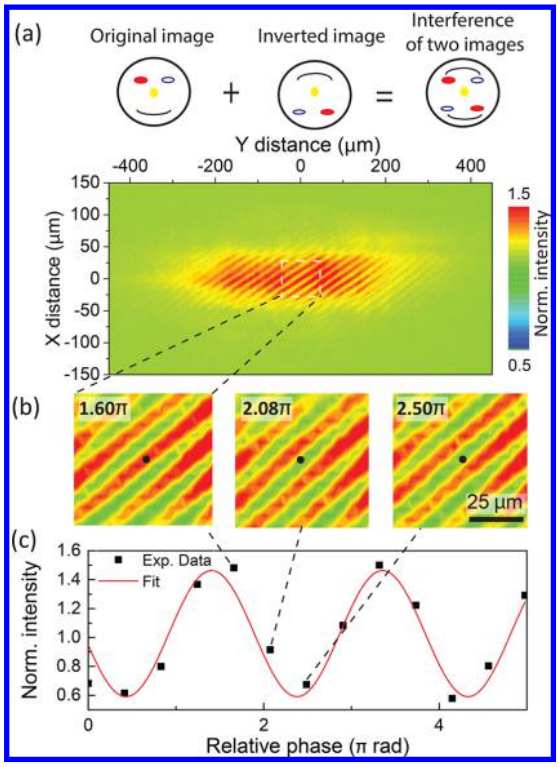

Figure 4. Spatial coherence and visibility. (a) Top: Illustration of the beam rotation where the real image on one arm of the interferometer was rotated centro-symmetrically after which the two images were overlapped on the camera. Bottom: Real-space image of the interference pattern at an excitation power of $P = 1.35\ P_{th}$. (b) Interferograms from the region indicated by the dashed white line in (a) at different phase delays. The black dot indicates a fixed position on the camera. (c) Interference fringe as a function of the relative phase, showing a contrast of ~45%. The red line is a cosine fit to the data. Interference fringes at different excitation densities are shown in Supporting Information Figure S2.

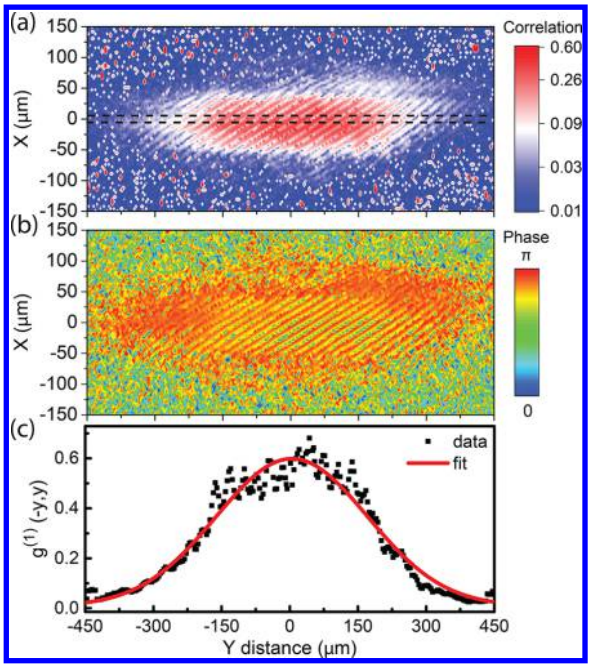

Figure 5. Long-range spatial coherence. (a) Map of the correlation function $g^{(1)}$ as a function of spatial position. Correlation values were obtained from cosine fits (as shown in Figure 4c) to the interference fringe from each pixel. (b) Extracted phase and (c) averaged $\langle g^{(1)} \rangle$ values from the region indicated by the two dashed lines in (a).

are shown in Figures 5a,b. Figure 5c displays the averaged $\langle g^{(1)} \rangle$ values from the region indicated by the two dashed lines in Figure 5a. By fitting this data using a Gaussian function where σ is the standard deviation, we extract an extraordinary long-range spatial coherence length[24] of $L = 2\sqrt{2\pi}\sigma = 0.904$ mm.

The large spatial coherence length observed in our measurements is surprising because it emerges spontaneously from a collection of nanoscale resonators. The individual nanodisks couple to each other through the index-matched solvent environment and the coherence length is substantially longer than the surface plasmon propagation length of thin films. The coherence emerges spontaneously as the pump excitation is nonresonant with the emission and the temporal coherence observed from the plasmon laser is even longer than for the pump laser itself. The observed coherence length of ~1 mm is significantly larger than even for BECs. Previously, spatial coherence has mostly been studied in BECs where coherence lengths up to ~40 μm have been observed.[23,24] The long-range spatial coherence observed in our system likely originates from the coherence intrinsic to the lattice plasmons, which is associated with the coupling between diffractive modes of the array and localized surface plasmons of the nanoparticles.[34] For high-quality lattice plasmon modes, all the nanoparticles in the array support charge oscillations with the same phase. Lasing based on this collective mode essentially has all the nanoparticles participating in a correlated manner (i.e., nanolaser arrays). Finally, we note that the periodicity of plasmon lattices has been shown to be crucial for the emergence of spatial coherence in both the weak and strong coupling limits and a spatial coherence length up to ~10 μm has been observed in the strong coupling regime.[31] However, for plasmonic cavity arrays, lasing has been shown to occur even with randomized lattices,[16] although the coherence properties of these systems have not been studied in detail. Similarly, we observed in our experiments that for nanoparticle arrays with many defects (i.e., damaged or missing nanoparticles as seen in dark field imaging), lasing emission still occurred; however, long spatial coherence was not detectable.

In summary, we have demonstrated for the first time the temporal and spatial long-range coherence characteristics from a nanostructured laser. Unlike other solid-state BECs or organic condensates, the lattice plasmon lasing based on nanoparticle arrays exhibits an extreme long-range spatial coherence even in the absence of strong coupling between the organic molecules and the lattice plasmon resonance. Such a long-range spatial coherent light source could be used as, for example, optical bridges for both inter- and intrachip communication. The simple design, operation, and tunability of this plasmon laser offers opportunities for new generations of devices that require on-chip tunable,[11] long-range spatially coherent light sources and offer a platform for studying the emergence of long-range coherence in plasmonic systems.

SAMPLE FABRICATION

Photoresist posts (diameter d = 120 nm; Shipley 1805) were first patterned in a square lattice (a_0 = 600 nm) on a Si (100) wafer using phase-shifting photolithography.[35] After deposition of a thin layer of Cr (8 nm) and lift-off of the photoresist, cylindrical pits (diameter ~120 nm and depth ~150 nm) were

DOI: 10.1021/acs.nanolett.7b02677
Nano Lett. 2017, 17, 6690−6695

generated by deep reactive ion etching beneath the circular Cr holes. Au nanohole arrays were then produced by depositing 100 nm Au and etching the sacrificial Cr layer. Next, Au nanohole arrays were floated onto fused silica substrates as deposition masks. Another Au deposition (h = 50 nm) and removal of the Au nanohole arrays by scotch tape left Au nanoparticle arrays on fused silica. The final arrays of nanoparticles had a dimension of approximately 5 × 5 mm. The lasing device was built by coating the Au nanoparticle arrays with a droplet of IR-140 (Sigma-Aldrich) dissolved in dimethyl sulfoxide (DMSO) which was stabilized with a piece of coverslip on top. The concentration of the dye was 1 mM, resulting in an average distance of ∼11 nm between molecules, and the thickness of the gain layer was ∼100 μm.

OPTICAL MEASUREMENTS

Angle-resolved transmission measurements were performed using a home-built setup. A broad-band white light source (Thorlabs SLS201) with a spot size of ∼2 mm was focused on the nanoparticle arrays. The sample with nanoparticle arrays was mounted on a rotation stage (0.1° resolution), and the transmitted light was collected through a multimode fiber, dispersed by a Horiba iHR550 spectrograph and detected using a Symphony CCD detector.

A mode-locked Ti:Sa laser (Coherent Libra, 1 kHz repetition rate, ∼ 150 fs pulse width) at 800 nm, spot size 1 mm, 45° incident angle was used for pumping the plasmonic lasing device. The photoluminescence of IR-140 was collected by a 5× and 34 mm working distance objective. The pump laser and photoluminescence signal were filtered by 800 nm band-pass and 820 nm long-pass filters (Semrock), respectively. The filtered photoluminescence was then coupled to a single-mode fiber and guided to the entrance slit of a spectrometer (Princeton Instrument SP2500) for spectral measurements or sent to a modified Michelson interferometer (in free space) for coherence measurements. The interference patterns were collected by a Hamamatsu CCD camera (C4742-80-12AG) every 100 ms (i.e., each image was averaged over 100 pulses). The motorized delay stage (Newport, model 850G) for moving the retroreflector and CCD camera were synchronized and controlled by a computer for data acquisition.

ASSOCIATED CONTENT

Supporting Information

The Supporting Information is available free of charge on the ACS Publications website at DOI: 10.1021/acs.nanolett.7b02677.

Photonic band structure measurements, excitation power dependence of coherence properties, and control measurements (PDF)

AUTHOR INFORMATION

Corresponding Author

*E-mail: m.mikkelsen@duke.edu. Phone: +1 (919) 660-0185.

ORCID

Teri W. Odom: 0000-0002-8490-292X

Maiken H. Mikkelsen: 0000-0002-0487-7585

Present Addresses

[#](T.B.H.) Department of Physics and Materials Science, The University of Memphis, Memphis, TN 38152.

[∇](A.Y.) Department of Materials Science and Engineering, Stanford University, Stanford, CA 94305.

Notes

The authors declare no competing financial interest.

ACKNOWLEDGMENTS

T.B.H, G.M.A., and M.H.M. acknowledge support from the Air Force Office of Scientific Research (AFOSR) Young Investigator Research Program (AFOSR, Grant FA9550-15-1-0301). A.Y. and T.W.O. acknowledge support from the National Science Foundation (NSF) under NSF Award Numbers DMR-1121262 and DMR-1608258.

REFERENCES

(1) Johnson, J. C.; Choi, H.-J.; Knutsen, K. P.; Schaller, R. D.; Yang, P.; Saykally, R. J. Single gallium nitride nanowire lasers. *Nat. Mater.* **2002**, *1* (2), 106−110.

(2) Duan, X.; Huang, Y.; Agarwal, R.; Lieber, C. M. Single-nanowire electrically driven lasers. *Nature* **2003**, *421* (6920), 241−245.

(3) Saxena, D.; Mokkapati, S.; Parkinson, P.; Jiang, N.; Gao, Q.; Tan, H. H.; Jagadish, C. Optically pumped room-temperature GaAs nanowire lasers. *Nat. Photonics* **2013**, *7* (12), 963−968.

(4) Ye, Y.; Wong, Z. J.; Lu, X.; Ni, X.; Zhu, H.; Chen, X.; Wang, Y.; Zhang, X. Monolayer excitonic laser. *Nat. Photonics* **2015**, *9* (11), 733−737.

(5) Altug, H.; Englund, D.; Vuckovic, J. Ultrafast photonic crystal nanocavity laser. *Nat. Phys.* **2006**, *2* (7), 484−488.

(6) Wu, S.; Buckley, S.; Schaibley, J. R.; Feng, L.; Yan, J.; Mandrus, D. G.; Hatami, F.; Yao, W.; Vuckovic, J.; Majumdar, A.; Xu, X. Monolayer semiconductor nanocavity lasers with ultralow thresholds. *Nature* **2015**, *520* (7545), 69−72.

(7) Nomura, M.; Kumagai, N.; Iwamoto, S.; Ota, Y.; Arakawa, Y. Laser oscillation in a strongly coupled single-quantum-dot-nanocavity system. *Nat. Phys.* **2010**, *6* (4), 279−283.

(8) Redding, B.; Choma, M. A.; Cao, H. Spatial coherence of random laser emission. *Opt. Lett.* **2011**, *36* (17), 3404−3406.

(9) Berini, P.; De Leon, I. Surface plasmon-polariton amplifiers and lasers. *Nat. Photonics* **2011**, *6* (1), 16−24.

(10) Zhou, W.; Dridi, M.; Suh, J. Y.; Kim, C. H.; Co, D. T.; Wasielewski, M. R.; Schatz, G. C.; Odom, T. W. Lasing action in strongly coupled plasmonic nanocavity arrays. *Nat. Nanotechnol.* **2013**, *8* (7), 506−511.

(11) Yang, A.; Hoang, T. B.; Dridi, M.; Deeb, C.; Mikkelsen, M. H.; Schatz, G. C.; Odom, T. W. Real-time tunable lasing from plasmonic nanocavity arrays. *Nat. Commun.* **2015**, *6*, 6939.

(12) Schokker, A. H.; Koenderink, A. F. Lasing at the band edges of plasmonic lattices. *Phys. Rev. B: Condens. Matter Mater. Phys.* **2014**, *90* (15), 155452.

(13) Nezhad, M. P.; Simic, A.; Bondarenko, O.; Slutsky, B.; Mizrahi, A.; Feng, L.; Lomakin, V.; Fainman, Y. Room-temperature subwavelength metallo-dielectric lasers. *Nat. Photonics* **2010**, *4* (6), 395−399.

(14) Stehr, J.; Crewett, J.; Schindler, F.; Sperling, R.; von Plessen, G.; Lemmer, U.; Lupton, J. M.; Klar, T. A.; Feldmann, J.; Holleitner, A. W.; Forster, M.; Scherf, U. A Low Threshold Polymer Laser Based on Metallic Nanoparticle Gratings. *Adv. Mater.* **2003**, *15* (20), 1726−1729.

(15) Suh, J. Y.; Kim, C. H.; Zhou, W.; Huntington, M. D.; Co, D. T.; Wasielewski, M. R.; Odom, T. W. Plasmonic Bowtie Nanolaser Arrays. *Nano Lett.* **2012**, *12* (11), 5769−5774.

(16) Schokker, A. H.; Koenderink, A. F. Statistics of Randomized Plasmonic Lattice Lasers. *ACS Photonics* **2015**, *2* (9), 1289−1297.

(17) Lu, Y.-J.; Kim, J.; Chen, H.-Y.; Wu, C.; Dabidian, N.; Sanders, C. E.; Wang, C.-Y.; Lu, M.-Y.; Li, B.-H.; Qiu, X.; Chang, W.-H.; Chen, L.-J.; Shvets, G.; Shih, C.-K.; Gwo, S. Plasmonic Nanolaser Using Epitaxially Grown Silver Film. *Science* **2012**, *337* (6093), 450−453.

DOI: 10.1021/acs.nanolett.7b02677
Nano Lett. 2017, 17, 6690−6695

(18) Hess, O.; Pendry, J. B.; Maier, S. A.; Oulton, R. F.; Hamm, J. M.; Tsakmakidis, K. L. Active nanoplasmonic metamaterials. *Nat. Mater.* **2012**, *11* (7), 573−584.
(19) Psaltis, D.; Quake, S. R.; Yang, C. Developing optofluidic technology through the fusion of microfluidics and optics. *Nature* **2006**, *442* (7101), 381−386.
(20) Bozhevolnyi, S. I.; Volkov, V. S.; Devaux, E.; Laluet, J.-Y.; Ebbesen, T. W. Channel plasmon subwavelength waveguide components including interferometers and ring resonators. *Nature* **2006**, *440* (7083), 508−511.
(21) Fischer, J.; Savenko, I. G.; Fraser, M. D.; Holzinger, S.; Brodbeck, S.; Kamp, M.; Shelykh, I. A.; Schneider, C.; Höfling, S. Spatial Coherence Properties of One Dimensional Exciton-Polariton Condensates. *Phys. Rev. Lett.* **2014**, *113* (20), 203902.
(22) Kasprzak, J.; Richard, M.; Kundermann, S.; Baas, A.; Jeambrun, P.; Keeling, J. M. J.; Marchetti, F. M.; Szymanska, M. H.; Andre, R.; Staehli, J. L.; Savona, V.; Littlewood, P. B.; Deveaud, B.; Dang, L. S. Bose−Einstein condensation of exciton polaritons. *Nature* **2006**, *443* (7110), 409−414.
(23) Daskalakis, K. S.; Maier, S. A.; Murray, R.; Kéna-Cohen, S. Nonlinear interactions in an organic polariton condensate. *Nat. Mater.* **2014**, *13* (3), 271−278.
(24) Daskalakis, K. S.; Maier, S. A.; Kéna-Cohen, S. Spatial Coherence and Stability in a Disordered Organic Polariton Condensate. *Phys. Rev. Lett.* **2015**, *115* (3), 035301.
(25) Plumhof, J. D.; Stöferle, T.; Mai, L.; Scherf, U.; Mahrt, R. F. Room-temperature Bose−Einstein condensation of cavity exciton−polaritons in a polymer. *Nat. Mater.* **2013**, *13* (3), 247−252.
(26) Väkeväinen, A. I.; Moerland, R. J.; Rekola, H. T.; Eskelinen, A. P.; Martikainen, J. P.; Kim, D. H.; Törmä, P. Plasmonic Surface Lattice Resonances at the Strong Coupling Regime. *Nano Lett.* **2014**, *14* (4), 1721−1727.
(27) Aberra Guebrou, S.; Symonds, C.; Homeyer, E.; Plenet, J. C.; Gartstein, Y. N.; Agranovich, V. M.; Bellessa, J. Coherent Emission from a Disordered Organic Semiconductor Induced by Strong Coupling with Surface Plasmons. *Phys. Rev. Lett.* **2012**, *108* (6), 066401.
(28) Rodriguez, S. R. K.; Feist, J.; Verschuuren, M. A.; Garcia Vidal, F. J.; Gómez Rivas, J. Thermalization and Cooling of Plasmon-Exciton Polaritons: Towards Quantum Condensation. *Phys. Rev. Lett.* **2013**, *111* (16), 166802.
(29) Liu, X.; Galfsky, T.; Sun, Z.; Xia, F.; Lin, E.-c.; Lee, Y.-H.; Kéna-Cohen, S.; Menon, V. M. Strong light−matter coupling in two-dimensional atomic crystals. *Nat. Photonics* **2014**, *9* (1), 30−34.
(30) Byrnes, T.; Kim, N. Y.; Yamamoto, Y. Exciton-polariton condensates. *Nat. Phys.* **2014**, *10* (11), 803−813.
(31) Shi, L.; Hakala, T. K.; Rekola, H. T.; Martikainen, J. P.; Moerland, R. J.; Törmä, P. Spatial Coherence Properties of Organic Molecules Coupled to Plasmonic Surface Lattice Resonances in the Weak and Strong Coupling Regimes. *Phys. Rev. Lett.* **2014**, *112* (15), 153002.
(32) Iwata, T.; Hieftje, G. M. Simple Method to Measure the Coherence Time of a Mode-Locked Laser. *Appl. Spectrosc.* **1992**, *46* (10), 1464−1468.
(33) Pusch, A.; Wuestner, S.; Hamm, J. M.; Tsakmakidis, K. L.; Hess, O. Coherent Amplification and Noise in Gain-Enhanced Nanoplasmonic Metamaterials: A Maxwell-Bloch Langevin Approach. *ACS Nano* **2012**, *6* (3), 2420−2431.
(34) Wang, D.; Yang, A.; Wang, W.; Hua, Y.; Schaller, R. D.; Schatz, G. C.; Odom, T. W. Band-edge engineering for controlled multi-modal nanolasing in plasmonic superlattices. *Nat. Nanotechnol.* **2017**, *12* (9), 889−894.
(35) Rogers, J. A.; Paul, K. E.; Jackman, R. J.; Whitesides, G. M. Using an elastomeric phase mask for sub-100 nm photolithography in the optical near field. *Appl. Phys. Lett.* **1997**, *70* (20), 2658−2660.

DOI: 10.1021/acs.nanolett.7b02677
Nano Lett. 2017, 17, 6690−6695